International Journal of Fatigue xxx (xxxx) 106676

Contents lists available at ScienceDirect

International Journal of Fatigue

journal homepage: www.elsevier.com/locate/ijfatigue

On the low-cycle fatigue behavior of thermo-mechanically processed high-strength aluminum alloys

S.V. Sajadifar [a,*], E. Scharifi [b], T. Wegener [a], M. Krochmal [a], S. Lotz [b], K. Steinhoff [b], T. Niendorf [a]

[a] University of Kassel, Institute of Materials Engineering, Mönchebergstraße 3, 34125 Kassel, Germany
[b] University of Kassel, Metal Forming Technology, Kurt-Wolters-Straße 3, 34125 Kassel, Germany

ARTICLE INFO

Keywords:
High-strength aluminum alloys
Low-cycle fatigue
Thermo-mechanical processing
Microstructure
Fracture

ABSTRACT

In present work low-cycle fatigue experiments were carried out on thermo-mechanically processed AA6082 and AA7075 sheets to evaluate mechanical properties under cyclic loading. Different cooling rates imposed by use of tempered forming tools after solutionizing, and subsequent aging treatment led to the formation of precipitates with differing sizes and morphologies. Specimens thermo-mechanically processed in tools with temperatures of 24 °C and 200 °C showed superior mechanical properties under both monotonic and cyclic loading. Significantly different behavior was observed for the specimens formed in the tool with a temperature of 350 °C. Based on thorough analysis of prevalent microstructural features, processing-property-damage relationships are established pointing at the major impact of the thermal history on the final performance of the high-strength aluminum alloys in focus.

1. Introduction

Excellent mechanical properties, e.g., high specific strength, good corrosion resistance and adequate ductility of high-strength aluminum alloys led to immense attention in academia and industry since decades [1–3]. Moreover, these alloys are utilized in various demanding engineering applications due to their outstanding strength-to-weight ratio, for example in aviation and automotive industry to replace steel components by much lighter parts [4–9]. To realize complex-shaped geometries such as hoods or trunks in these fields, thin-walled sheet materials have to undergo complex stress–strain-paths during traditional forming processes, eventually leading to pronounced springback and local material thinning, the latter due to the limited formability of high-strength aluminum alloys in particular at room temperature. For this reason, different forming techniques exploiting high temperatures were introduced to overcome these challenges [10–12]. One of the promising techniques combines hot forming and quenching within a single forming tool after initial solution heat treatment [10,13]. This forming process enables the production of complex-shaped components of high strength aluminum alloys being characterized by minimized springback and high dimensional accuracy [14–15].

The above-mentioned approach also offers high potential for use in aerospace industry to form complex shaped aluminum structures. In this regard, Gao et al. utilized this technique for forming of wing stiffener components made of AA2060 alloy [14]. For this propose, hot stamping was carried out in two steps, where the first step aimed at forming of the desired geometry at 470 °C and the second step performed the final heat treatment to establish mechanical properties similar to those in the T6-condition. As shown, forming of high strength aluminum alloys at elevated temperatures promotes much higher formability compared to room temperature forming upon optimization of the temperature–time history during processing. Concerning the above mentioned thermo-mechanical process, the cooling rate of the sheet material after solutionizing can be controlled by the tool temperature [16–19].

So far, different tool temperatures were employed to set various cooling rates and, thus, different mechanical properties in the final parts in case of AA6082 and AA7075 alloys [16,20–22]. On the one hand, lower tool temperatures resulted in a higher cooling rate and, hence, the formation of fine and dispersed precipitates during subsequent aging treatment. These fine and dispersed precipitates are capable of hampering dislocation slip and eventually increase the strength of the treated material [21]. On the other hand, higher tool temperatures caused a lower cooling rate and, thus, the formation of coarse precipitates along the grain boundaries. These coarse precipitates and concomitant precipitate-free zones (PFZs) were found to be detrimental with respect to the intended strengthening of AA6082 and AA7075 alloys [16,23].

* Corresponding author.
E-mail address: sajjadifar@uni-kassel.de (S.V. Sajadifar).

https://doi.org/10.1016/j.ijfatigue.2021.106676
Received 15 October 2021; Accepted 25 November 2021

Many studies have focused on the mechanical properties of high-strength aluminum alloys under cyclic loading [2,24,33–34,25–32]. In some of the previous studies, severe plastic deformation as a novel thermo-mechanical processing route was employed to increase the strength and fatigue resistance of aluminum alloys [2,26]. Generally, grain refinement was reported to improve the resistance of the microstructure against crack initiation. On the contrary, grain refinement was shown to have detrimental effects on the crack growth rate [35–36]. Besides, the influence of cold deformation on the cyclic response of aluminum alloys was probed by symmetrical and asymmetrical rolling [31–32]. A cold rolling process was applied on an AA7050 alloy to enhance its fatigue performance [31]. Symmetrical rolling process were shown to result in higher fatigue life compared to the asymmetrical rolling [31,37]. Better resistance to crack initiation in the symmetrical rolled specimens stemmed from the formation of subgrains in the near-surface layers [31]. In another work the effect of cold deformation on the cyclic properties was studied by applying pre-strains up to 8% on the AA7050 in the T6 state [32]. Results shown indicate that such specific pre-strain histories reduce fatigue life. A noticeable improvement in low-cycle fatigue (LCF) life was achieved via ultrasonic shot peening [33]. Ultrasonic shot peening introduced compressive residual stresses being very effective in improving the performance of components under cyclic loading. Similarly, compressive residual stresses introduced by laser peening were found to postpone fatigue crack initiation and decelerate the fatigue crack growth rate [38].

Furthermore, the impact of various heat treatments and related precipitation processes on the cyclic behavior of aluminum alloys was analyzed [29–30,34,39]. In one of these studies the effect of different aging conditions on the high-cyclic fatigue (HCF) behavior of AA7075 alloy was explored [29]. Obtained results reveal that peak aged specimens exhibit the highest fatigue strength. Formation of fine and dispersed precipitates was claimed to be the main reason for the improvement of fatigue properties in this alloy. In another study, aging of AA6063 alloy at temperatures between 160 °C and 200 °C for 7 to 9 h led to an optimal fatigue performance [30]. It was also shown that fine precipitates can improve the properties of AA6061 and AA2024 alloys under cyclic loading [34,39]. However, the growth of the formed precipitates imposed by a higher aging temperature adversely affected the fatigue behavior of these alloys.

Only a very limited number of studies analyzed the effect of precipitate sizes and morphologies on the cyclic properties of thermo-mechanically processed high-strength aluminum alloys so far. Cyclic mechanical properties of tool quenched AA6082 and AA7075 alloys have not been reported, yet. In order to close this gap, the present paper intends to contribute to a better understanding of the mechanisms related to thermo-mechanical processing of two different aluminum alloys, i.e., AA6082 and AA7075, and their effects on the fatigue performance. Here, fatigue performance of thermo-mechanically processed aluminum alloys was studied in the LCF regime under a wide range of total strain amplitudes. Mechanical behavior and fatigue properties of the thermo-mechanically processed aluminum alloys are discussed based on evaluation of half-life hysteresis curves, Masing behavior and fracture surface analysis. Data obtained are used to establish relationships between fatigue strength, fatigue life and the microstructural appearance of the precipitation-hardened region in the thermo-mechanically processed parts. Results of present work will be very helpful to tailor mechanical properties and microstructure of high-strength aluminum alloys in application.

2. Experimental procedure

Sheets of AA6082 and AA7075 were delivered in T6 state by BIKAR-METALLE and AMAG, respectively. The chemical compositions listed in Table 1 were characterized by the optical emission spectroscopy (OES) technique.

Sheets of both alloys were cut into blanks of 250 mm × 140 mm × 1.5 mm. A schematic detailing the subsequent steps accomplished in thermo-mechanical processing is shown in Fig. 1.

Table 1
Chemical compositions of aluminum alloys studied in present work.

Alloy	Si	Fe	Cu	Mn	Mg	Cr	Zn	Ti	Zr	Al
AA6082 (wt.-%)	0.90	0.42	0.10	0.44	0.80	0.02	0.19	0.04	–	Balance
AA7075 (wt.-%)	0.10	0.11	1.49	0.03	2.38	0.20	5.57	0.03	0.04	Balance

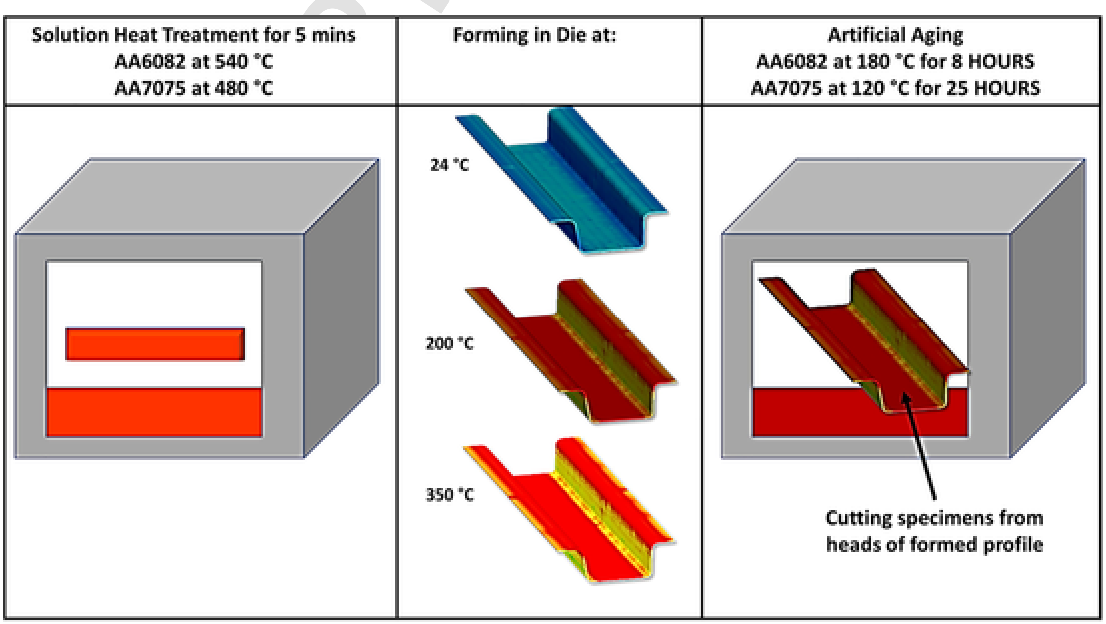

Fig. 1. Schematic highlighting the relevant steps for the thermo-mechanical processing route employed in the present study.

The blanks were firstly solution heat treated for 5 min and then directly transferred to the forming tool. The blanks of both alloys were formed in tools with different temperatures (24 °C, 200 °C and 350 °C). Upon forming, the profiles were finally aged in a furnace. Details related to thermo-mechanical processing and the forming steps can be found in [16].

From the heads of formed profiles, tensile and fatigue specimen were cut using electro-discharge machining (EDM). Tensile and fatigue specimens were ground via SiC abrasive papers beforehand to remove recast layers due to the EDM. Tensile experiments were performed on specimens with nominal gauge section dimensions of 50 mm × 12.5 mm × 1.5 mm. Three tensile tests for each condition were carried out. Tensile tests were conducted using a Hegewald & Peschke screw driven tensile testing machine at room temperature with a nominal crosshead speed of 5 mm min^{-1}. LCF experiments were carried out on miniature dog-bone shaped specimens with nominal gauge section dimensions of 8 mm × 3 mm × 1.5 mm. Such type of specimens has already often been used in literature for similar investigations [40–43]. An MTS servo-hydraulic test rig was used to perform the fatigue experiments. All LCF experiments were conducted at room temperature under a nominal strain rate of 0.006 s^{-1} under strain-control in fully reversed push–pull loading (R = −1). LCF tests were carried out at three total strain amplitudes of $\Delta\varepsilon_t/2$ = 0.2%, 0.4% and 0.6%. A MTS miniature extensometer featuring a gauge length of 5 mm was utilized to measure the strain during LCF testing. Three LCF tests per strain amplitude were performed to evaluate repeatability of experiments. As cyclic deformation responses (CDRs) were very similar, only one plot for each condition is displayed for the sake of brevity in the following chapter.

A scanning electron microscope (SEM) (CamScan MV 2300) was employed to analyze the microstructure and fracture surface morphologies of the specimens. The SEM was operated at a nominal accelerating voltage of 20 kV. For back-scatter electron (BSE) imaging, specimen were ground down to to 5 μm grit size using SiC papers followed by polishing in a colloidal silica solution with the particle size of 0.05 μm.

3. Results and discussion

3.1. Microstructure of thermo-mechanically processed AA6082 and AA7075 alloys

Representative BSE images of the differently thermo-mechanically processed AA6082 and AA7075 alloys are shown in Fig. 2. Formation of coarse precipitates in the AA7075 specimen formed in the heated forming tool at 350 °C is evident, while specimens processed in the tool with a temperature of 24 °C are characterized by the presence of fine and dispersed precipitates. The higher cooling rate induced by the cold tool suppresses the nucleation of precipitates during cooling [16,20,23,44–45]. The reader is referred to [16,46] for further in-depth microstructure characterization upon thermo-mechanical processing. In previous work focusing on the same conditions, a comprehensive microstructural analysis of the thermo-mechanically processed AA6082 and AA7075 alloys using different techniques, i.e., energy dispersive spectroscopy (EDS), electron backscatter diffraction (EBSD) and scanning transmission microscopy (STEM) was reported [16,46]. In those studies it already was shown that the impact of the different thermo-mechanical processing routes considered here on the finally prevailing grain sizes is low.

3.2. Mechanical properties under monotonic loading

Tensile properties under quasistatic loading of the thermo-mechanically processed AA6082 and AA7075 alloys were also reported in the authors' previous research work [16]. However, as a basis for solid understanding of the most important underlying mechanisms during cyclic loading of these alloys, it is important to briefly report and reassess data. The tensile properties of AA6082 and AA7075 upon different thermo-mechanically processes are provided in Table 2. Specimens formed and quenched in tools with temperatures of 24 °C and 200 °C exhibit yield strength (YS) and ultimate tensile strength (UTS) almost as high as in the T6 condition. On the contrary, forming in the heated tool at 350 °C caused deterioration of strength in both alloys. Changes in mechanical properties with varying tool temperatures can be rational-

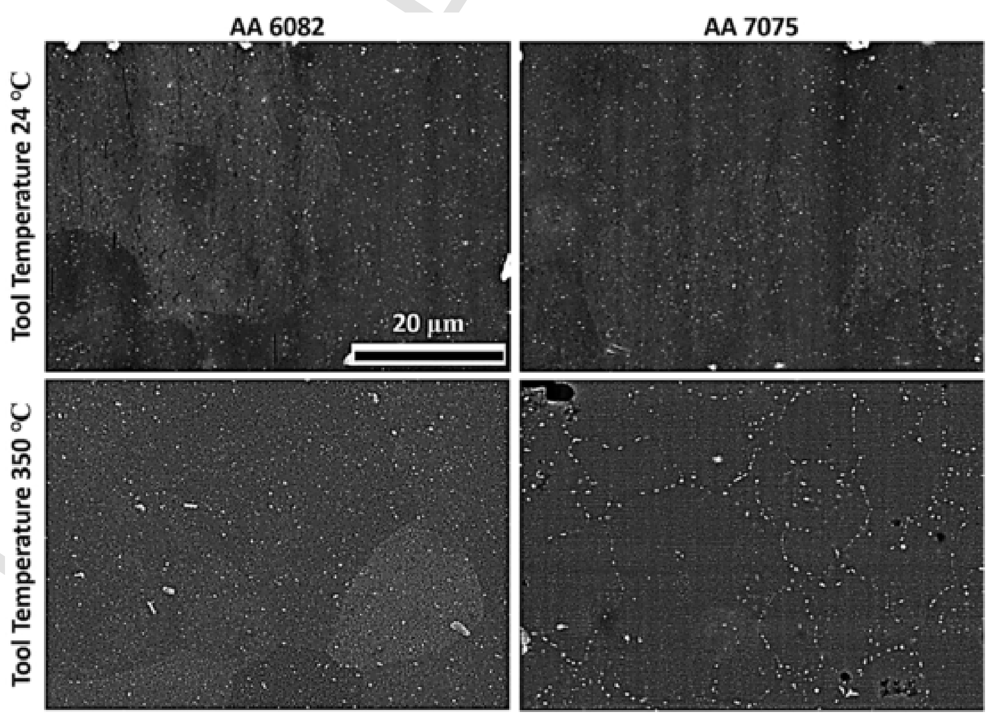

Fig. 2. BSE images detailing microstructure evolution for differently thermo-mechanically processed AA6082 and AA7075 alloys highlighting changes in precipitation kinetics as a function of cooling rates.

Table 2
Tensile properties of differently thermo-mechanically processed AA6082 and AA7075 alloys. Standard deviations are provided in the table (partly recompiled from [16]).

Alloy	AA6082			AA7075		
Conditions	YS (MPa)	UTS (MPa)	Elongation (%)	YS (MPa)	UTS (MPa)	Elongation (%)
As-received (T6)	310 ± 4	340 ± 6	14.1 ± 1	470 ± 4	580 ± 5	14.3 ± 1
Tool temperature 24 °C	319 ± 5	338 ± 8	7 ± 3	489 ± 8	576 ± 6	10.4 ± 2
Tool temperature 200 °C	302 ± 4	330 ± 5	11.2 ± 3	490 ± 10	561 ± 8	11.2 ± 5
Tool temperature 350 °C	79 ± 3	163 ± 6	15.9 ± 2	164 ± 8	338 ± 9	13.9 ± 3

ized based on different kinetics of precipitation. In previous work it was shown that fine and well-dispersed precipitates in the specimen formed and quenched in the cold tool are responsible for the increase in strength under monotonic loading [16,46]. On the contrary, coarsening of precipitates, grain boundary decoration, and concomitant evolution of PFZs were found to be detrimental.

3.3. Mechanical properties under cyclic loading

All fatigue tests addressed the LCF regime. CDRs of the thermo-mechanically processed AA6082 and AA7075 alloys are shown in Fig. 3. It is well-accepted that the LCF regime considers tests up to about 10^5 cycles [47] and, thus, specimens exceeding 150,000 cycles without failure are reported as runouts in the present study. All specimen fatigued at the lowest total strain amplitude ($\Delta\varepsilon_t/2 = 0.2\%$) except the AA6082 condition formed in the tool with a temperature of 350 °C could withstand more than 150,000 cycles. Regardless of tool temperature, stress amplitude increases with an increase in the total strain amplitude in both alloys. Concomitantly, fatigue lives of both alloys reduced with the increase of the total strain amplitude. At higher total strain amplitudes, specimens suffer more rapid fatigue crack initiation and propagation [48–49]. It should also be noted that at higher $\Delta\varepsilon_t/2$, stress levels of AA7075 alloy are always higher than those of AA6082 alloy. This can be attributed to the higher resistance toward dislocation slip and plasticity, respectively, in the AA7075 alloy, being already seen in its higher YS compared to that of AA6082 alloy under quasistatic tensile testing.

Focusing on the effect of thermo-mechanical processing, specimens formed and quenched in tools with temperatures of 24 °C and 200 °C are characterized by stress amplitudes close to those in the as-received (T6) condition. A different behavior was observed during cyclic loading of the specimens formed in the tool with a temperature of 350 °C. For a given total strain amplitude, stresses of specimens formed in the tool with a temperature of 350 °C are considerably lower than those of the T6 condition and specimens formed in the tools with lower temperatures. It is well-documented in literature that morphologies and sizes of precipitates can affect not only the monotonic strength of high-strength aluminum alloys under monotonic loading but also their fatigue strength [29,34]. Adequately shaped fine and dispersed precipitates improve the strength of these alloys in general and even can improve their resistance to fatigue crack initiation. However, strain localization induced by cutting of precipitates being to small needs to be avoided [50–52]. Coarse precipitates present in the specimen formed in the tool with a temperature of 350 °C result in a large interparticle spacing facilitating dislocation slip and formation of dislocation cell walls and substructures [53–54]. However, fine and disperse precipitates in the parts formed in the tools with temperatures of 24 °C and 350 °C cause a low interparticle spacing signifying dislocation-precipitate interactions. Therefore, different fatigue performances (e.g. fatigue life and strength) of differently thermo-mechanically processed AA6082 and AA7075 alloys can be linked to the interparticle spacing leading to either dislocation-precipitate interactions or dislocation–dislocation interactions. These aspects are discussed in detail in the chapter 3.5 of the present work.

Another aspect to be considered in evaluation of the CDRs of thermo-mechanically processed AA6082 and AA7075 is the cyclic hardening/softening behavior during LCF testing. It should be noted that strains were increased stepwise in the first 10–25 cycles depending on the actual total strain amplitude in order to prevent buckling of the miniature specimens. Therefore, strain hardening in the course of the

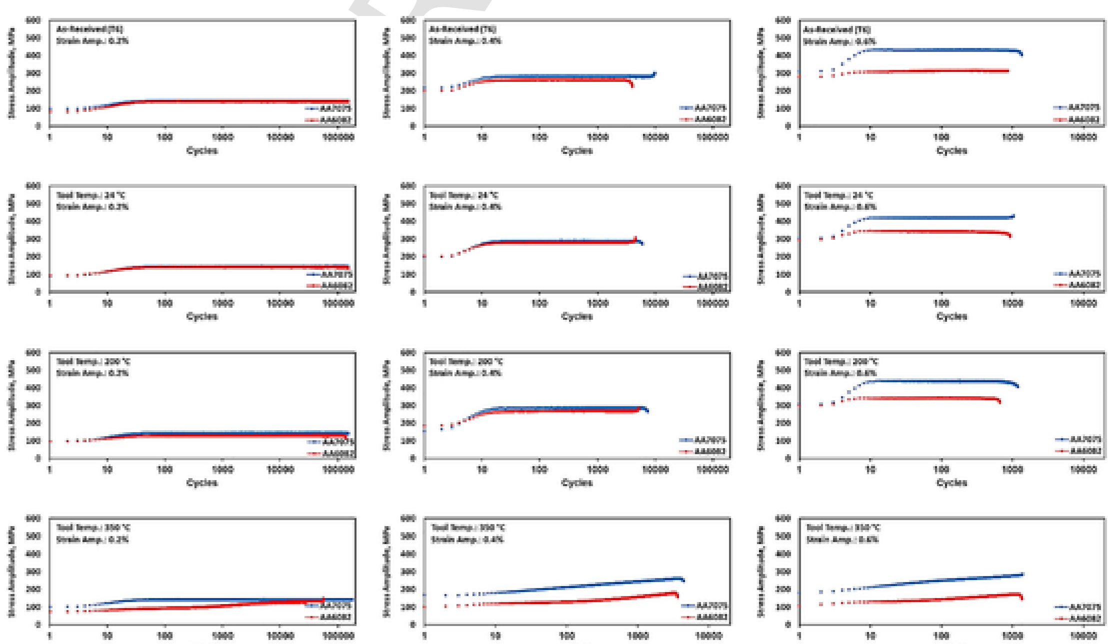

Fig. 3. CDRs of AA6082 and AA7075 alloys in different conditions. Information on the actual condition and the strain amplitude are provided in the upper left of each subimage.

first 50 cycles may not be directly related to the intrinsic material behavior. Specimens formed in tools with temperatures of 24 °C and 200 °C exhibit neither hardening nor softening. As-received (T6) specimens also show a saturation stage similar to the conditions formed in the cold tool. A lack of softening/hardening is an indication of predominant elastic deformation (at the global scale) and/or simultaneous generation and cancellation of dislocations [48,55]. Furthermore it can be directly deduced that neither cutting of precipitates and strain localization nor evolution of dislocation cell structures take place [52,56]. Specimens formed in the tool with a temperature of 350 °C exhibit steady cyclic hardening during LCF testing (with the exception of the AA7075 at lowest strain amplitude). This can be attributed to a progressive dislocation generation and dislocation–dislocation as well as dislocation precipitate interactions during cyclic loading, eventually leading to the evolution of dislocation cell structures in between the coarsened precipitates [52,56–59]. At this point further in-depth analysis requires assessment of microstructure evolution via transmission electron microscope (TEM), which is beyond the scope of the present study.

Half-life hysteresis loops of AA6082 and AA7075 alloys in various conditions are displayed in Fig. 4. In many cases merely elastic deformation is seen, i.e., hysteresis curves remain fully closed. In case of significant contribution of plastic strain, half-life hysteresis loops of both alloys remain relatively symmetrical. Since slip during cyclic plastic straining is the dominant deformation mechanism in face-centered cubic (fcc) metals, symmetrical loops are often seen during LCF testing [39,52]. The areas of hysteresis loops are an indication of the relevant energy dissipation per cycle [60–61]. The as-received (T6) specimens of AA7075 alloy and the ones formed in the tools with temperatures of 24 °C and 200 °C show very narrow hysteresis loops for all examined total strain amplitudes. At $\Delta\varepsilon_t/2$ of 0.2% and 0.4%, T6 specimens of AA6082 alloy and the ones formed in the tools with temperatures of 24 °C and 200 °C also exhibit narrow hysteresis loops, attesting an almost fully elastic deformation response during cyclic loading. However, wide opened loops were obtained for the specimen of both alloys formed in the tool with a temperature of 350 °C revealing a significant contribution of plastic deformation during cycling. It is also worth noting that at the highest total strain amplitude (0.6%), the loops of AA6082 alloy are wide opened in all conditions. AA6082 specimen have lower YS than AA7075 counterparts and, thus, plastic behavior during cyclic deformation at the higher total strain amplitude is to be expected for this alloy.

For further assessment of the thermo-mechanically processed AA6082 and AA7075 alloys under cyclic loading, half-life hysteresis loops of both alloys are plotted in relative coordinates (Fig. 5). Masing/Non-Masing behavior of AA7075 specimens formed in the tools with temperatures of 24 °C and 200 °C can hardly be traced as they are characterized by narrow and elastic hysteresis loops at all examined total strain amplitudes. AA6082 specimens formed in the tools with temperatures of 24 °C and 200 °C show Masing behavior. On the contrary, specimen of both alloys formed in the tool with a temperature of 350 °C exhibit Non-Masing behavior. This fact clearly indicates remarkable changes in the microstructure during cyclic loading. Non-Masing behavior is an indication of severe dislocation activities, i.e., dislocation multiplication and their re-arrangement due to the cyclic plastic deformation [55,62–63]. It is known for fcc alloys being characterized by wavy slip that dislocation cell structures can form being different in size depending on the actual loading amplitude [52,56]. In precipitation hardened fcc alloys such behavior can be suppressed when dislocation-

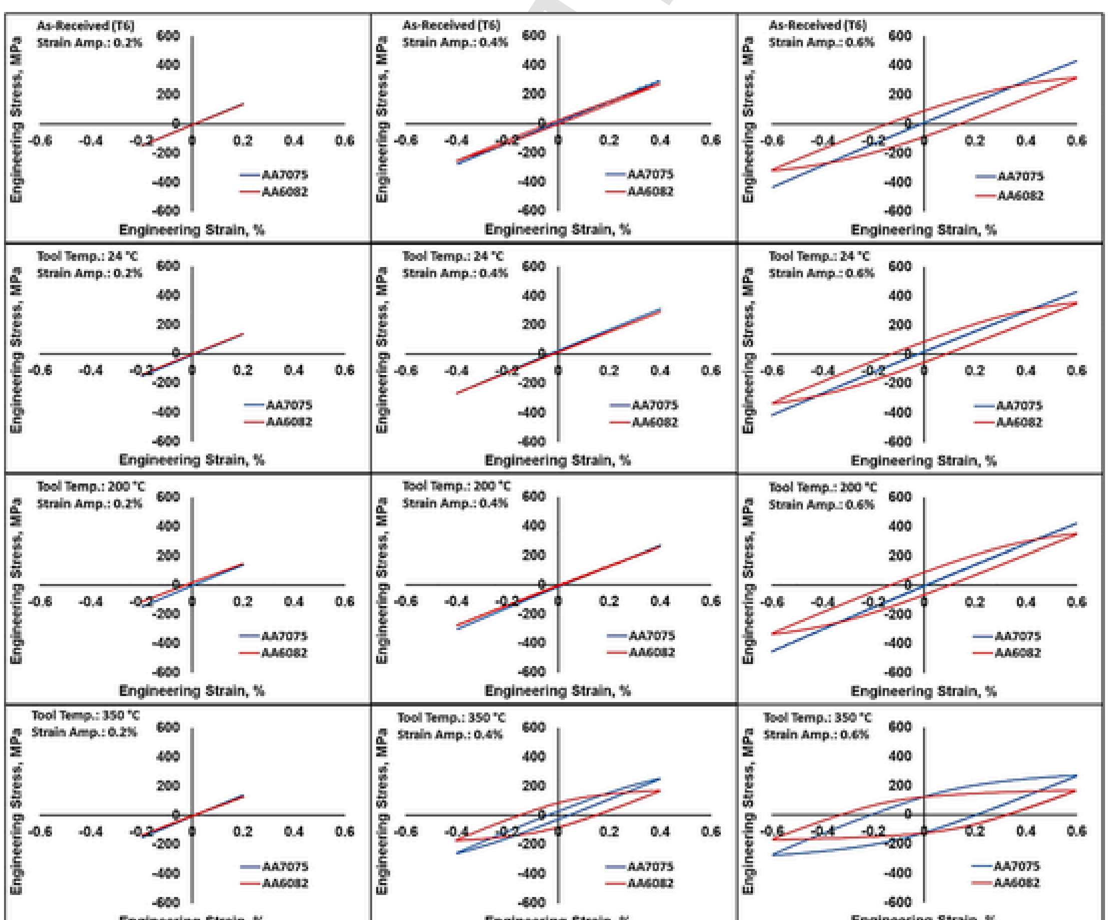

Fig. 4. Half-life hysteresis loops of AA6082 and AA7075 alloys in different conditions. Information on the actual condition and the strain amplitude are provided in the upper left of each subimage.

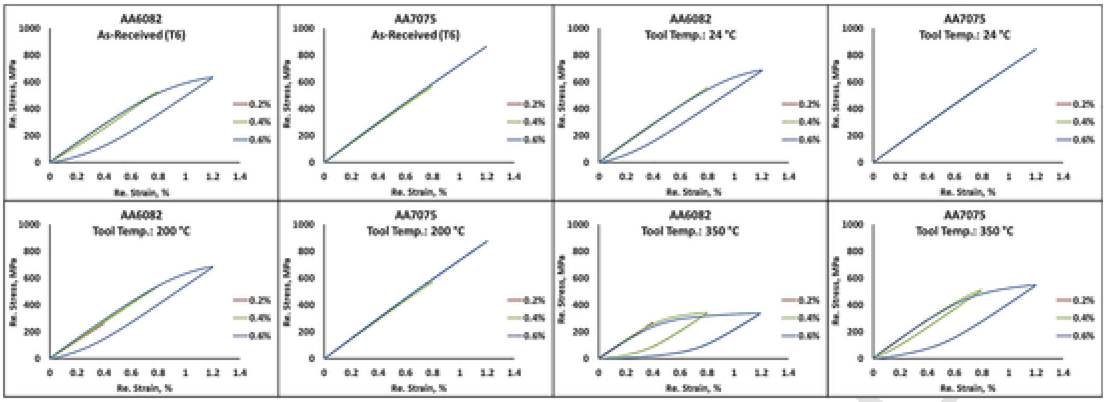

Fig. 5. Half-life hysteresis loops of AA6082 and AA7075 alloys in different conditions plotted in relative coordinates of stress and strain.

precipitate interactions dominate the overall deformation response. This seems to be the case in all conditions encountering rapid cooling upon solutionizing, i.e., all conditions processed in the cold tools. As has been detailed before, precipitation kinetics are different upon quenching in the tool at 350 °C. The coarse precipitate structure eventually allows for the evolution of the dislocation cell structures, at least in specimen volumes being characterized by large precipitate-precipitate distances [52,56]. Finally, dependent on the actual strain amplitude differences in dislocation cell structures prevail leading to the Non-Masing behavior seen in Fig. 5. As already mentioned before, experimental proof will require in-depth TEM analysis being out of the scope of present work.

3.4. Fractography

Fracture surfaces of AA6082 and AA7075 alloys in various conditions upon LCF testing are displayed in Fig. 6. From Fig. 6, it can be deduced that the initiation sites of fatigue cracks always stem from near-surface defects. Generally, fatigue crack can nucleate in the bulk or surface depending on various parameters, e.g., fatigue regime, material condition, concentration of internal defects, processing history and surface treatment [64–65]. Underlying mechanisms for the initiation of fatigue cracks at the surface are discussed in the following section. Generally, the fatigue crack propagation area is reduced upon increase of the total strain amplitude. This behavior was numerously reported for LCF testing of other materials [39,55,66]. At higher magnification, microc-

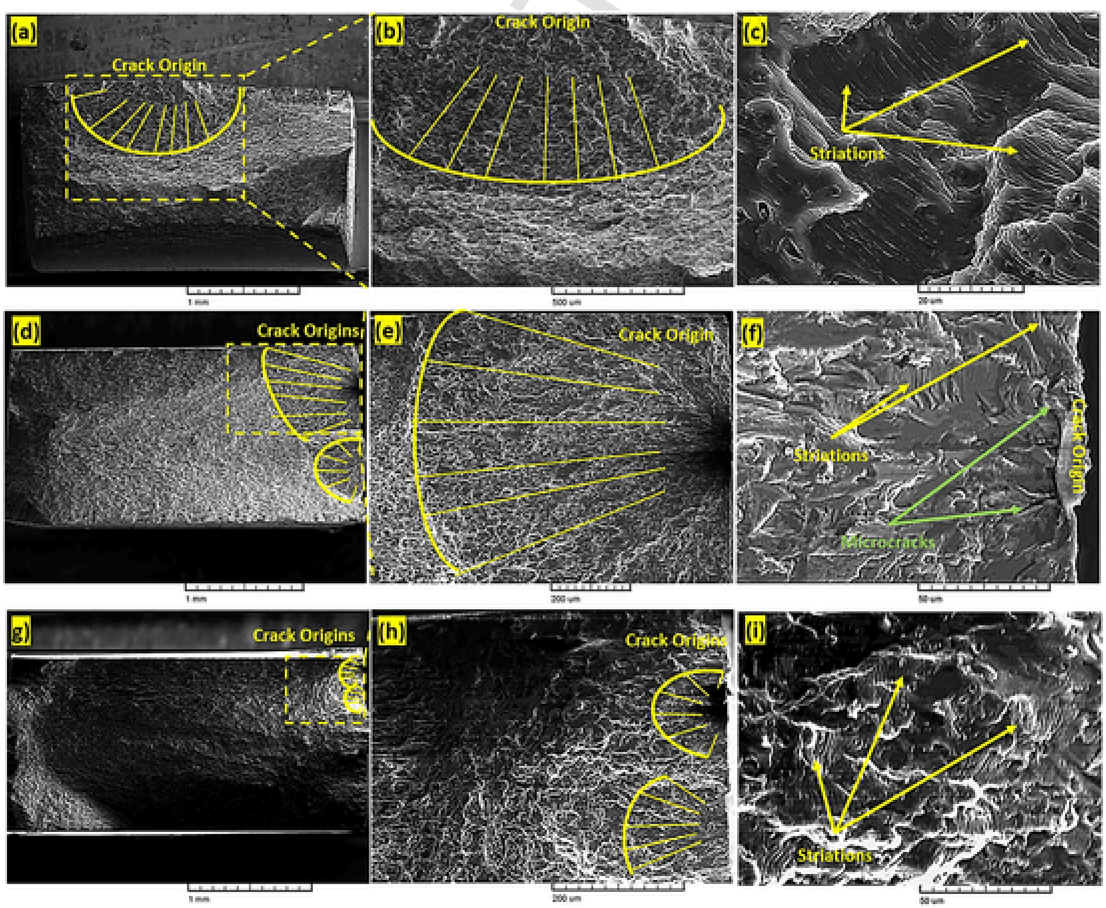

Fig. 6. Fracture surfaces of (a–c) AA6082 specimen formed in tool with temperature of 350 °C and fatigued at 0.6%, (d–f) AA7075 as-received specimen fatigued at 0.4%, (g–i) AA7075 as-received specimen fatigued at 0.6%; higher magnifications of fracture are displayed to the right.

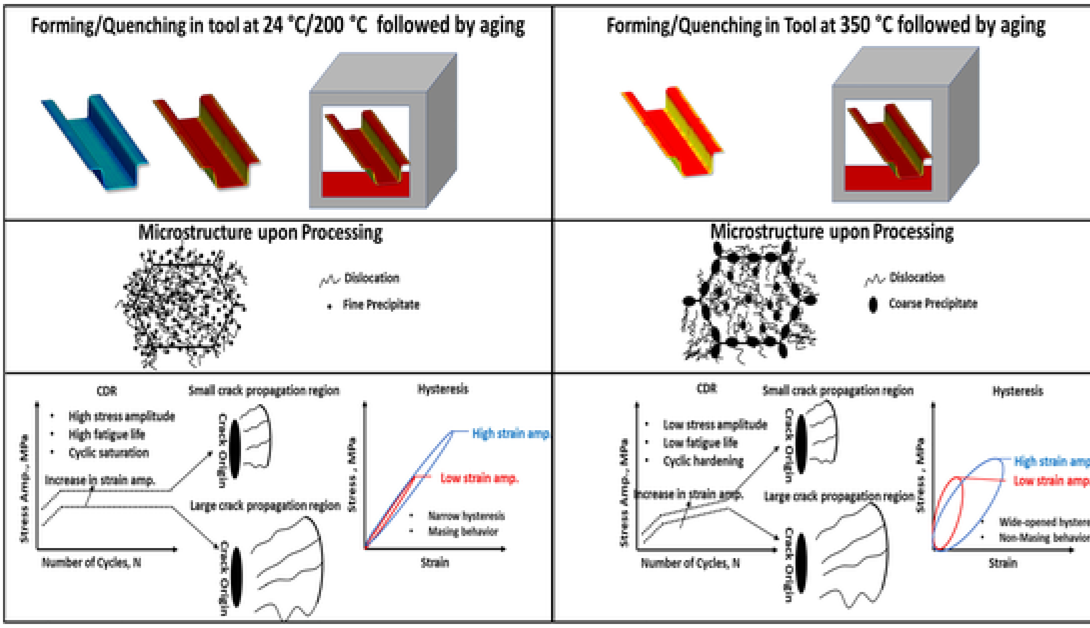

Fig. 7. Schematic illustration highlighting changes in microstructure and fatigue properties imposed by quenching and forming at different tool temperatures.

racks and striations can be assessed as an indication of the locally prevailing fatigue crack propagation rate [67–69]. By analyzing numerous fracture surfaces it was found that the different tool temperatures only have a minimum effect on the fracture morphologies of the specimen fatigued at various strain amplitudes. Thus, only representative micrographs detailing important features for analysis of damage evolution are shown in Fig. 6 for brevity.

3.5. Process-microstructure-property-damage relationships

The process-microstructure-property-damage relationships derived from the results shown are schematically illustrated in Fig. 7. As elaborated in the authors' previous studies [16,20,23], forming/quenching specimens in tools with temperatures of 24 °C and 200 °C causes the introduction of fine and disperse precipitates, whereas forming specimens in the tool with a temperature of 350 °C promotes the formation of coarse precipitates.

The effects of precipitate morphologies and sizes on the fatigue performances of both alloys were already discussed above. Specimens formed in the tools with temperatures of 24 °C and 200 °C showed neither cyclic hardening nor cyclic softening. This can be rationalized in terms of dislocation–dislocation and dislocation-precipitate interactions. It was found that for the aluminum alloys containing fine and dispersed precipitates, e.g., in T6 condition, interparticle spacing is low and, hence, the formation of dislocation cell walls and subgrains cannot occur during cyclic deformation [53–54]. Results obtained in present work indicate that during cyclic deformation of the specimens formed and quenched in the cold tools, dislocation-precipitate interactions are more dominant than dislocation–dislocation interaction. However, larger interparticle spacing in the specimens formed in the tool with a temperature of 350 °C signifies dislocation–dislocation interactions under cyclic deformation. The dislocation cell shuttling mechanism was mentioned to be the underlying mechanism for cyclic hardening in aluminum alloys, where dislocation–dislocation interactions are dominant, e.g., in overaged conditions [58,70–71]. Based on this mechanism, screw dislocations are bowed to develop loops in the cell walls towards the cell interior. Considering this mechanism considerable changes in the microstructure are expected, rationalizing the observed Non-Masing behavior of the specimens formed in the tool with a temperature of 350 °C. It should also be noted that wide opened hysteresis loops of formed specimens in the heated tool indicate high energy dissipation per cycle. The energy dissipation in this case can be a factor further promoting the dislocation interactions detailed before.

Considering observations of fracture analysis, it can be deduced that fatigue cracks initiated mostly at near-surface defects as pointed out earlier. Pores and inclusions were found to be responsible for the nucleation of near-surface cracks [72]. Serrano-Munoz et al. studied the location of fatigue crack initiation in Al-Si cast alloys [73]. Their results suggest that during cyclic loading an internal defect should be at least three times larger than surface or near-surface ones to be able to promote subsurface nucleation of a fatigue crack. Therefore, the presence of defects even in small sizes at the surface is very detrimental for the fatigue life of components. It is also worth noting that surface defects can be introduced during cyclic deformation [74]. In the LCF regime, cyclic slip irreversibility at the surface can also trigger crack nucleation [74–76]. During forward loading, some dislocations reach the surface of the material and then they never return to the specimen interior in the reverse loading direction, eventually leaving irreversible slip behind. Accumulation of cyclic slip irreversibility leads to local stress concentration at the surface and eventually initiation of cracks from those points.

4. Summary and conclusions

Fatigue performance of thermo-mechanically processed AA6082 and AA7075 alloys was explored by conducting LCF experiments at three strain total amplitudes of $\Delta\varepsilon_t/2 = 0.2\%$, 0.4% and 0.6%. The most significant findings of present work can be summarized as follows:

i. Fatigue strength and life strongly depend on the tool temperature in the forming and quenching process used in the present study. Forming both alloys in the cold tool resulted in superior fatigue properties stemming from fine and dispersed precipitates compared to coarse precipitate structures formed in the tool at a temperature of 350 °C.
ii. Half-life hysteresis loops revealed that specimens processed in tools with temperatures of 24 °C and 200 °C are characterized by narrow loops and small hysteresis areas, while loops of specimens formed in the tool with a temperature of 350 °C demonstrated a wide opened hysteresis.

iii. Specimens formed in the tool with a temperature of 350 ˚C showed Non-Masing behavior indicating considerable dislocation generation and activities during cyclic loading. Fatigue properties obtained in the present work suggest that interparticle spacing is a very important parameter for the designation of mechanical properties of high-strength aluminum alloys under cyclic loading. Low interparticle spacing in the parts formed in the cold tool can inhibit the formation of substructures, while larger interparticle spacing in the components formed in the tool with a temperature of 350 ˚C may allow the formation of subgrains and dislocation cells.

Declaration of Competing Interest

The authors declare that they have no known competing financial interests or personal relationships that could have appeared to influence the work reported in this paper.

Acknowledgements

The authors would like to thank financial support from the Hessen State Ministry for Higher Education, Research and the Arts – Initiative for the Development of Scientific and Economic Excellence (LOEWE) for the project *ALLEGRO* (Subprojects A2 and B1). Moreover, the authors want to thank Mr. Dipl.-Ing. Stefan Seidel for sample preparation.

References

[1] Cepeda-Jiménez CM, García-Infanta JM, Ruano OA, Carreño F. Mechanical properties at room temperature of an Al–Zn–Mg–Cu alloy processed by equal channel angular pressing. J Alloys Compd 2011;509(35):8649–56. https://doi.org/10.1016/j.jallcom.2011.06.070.

[2] Hockauf K, Wagner M-F-X, Halle T, Niendorf T, Hockauf M, Lampke T. Influence of precipitates on low-cycle fatigue and crack growth behavior in an ultrafine-grained aluminum alloy. Acta Mater 2014;80:250–63. https://doi.org/10.1016/J.ACTAMAT.2014.07.061.

[3] Jayaganthan R, Brokmeier H-G, Schwebke B, Panigrahi SK. Microstructure and texture evolution in cryorolled Al 7075 alloy. J Alloys Compd 2010;496(1–2):183–8. https://doi.org/10.1016/j.jallcom.2010.02.111.

[4] Tisza M, Czinege I. Comparative study of the application of steels and aluminium in lightweight production of automotive parts. Int J Light Mater Manuf 2018;1(4):229–38. https://doi.org/10.1016/j.ijlmm.2018.09.001.

[5] Liu Y, Zhu Z, Wang Z, Zhu B, Wang Y, Zhang Y. Formability and lubrication of a B-pillar in hot stamping with 6061 and 7075 aluminum alloy sheets. Procedia Eng 2017;207:723–8. https://doi.org/10.1016/J.PROENG.2017.10.819.

[6] Harrison NR, Luckey SG. Hot Stamping of a B-Pillar Outer from High Strength Aluminum Sheet AA7075. SAE Int J Mater Manuf 2014;7(3):567–73. https://doi.org/10.4271/2014-01-0981.

[7] Starink MJ. Effect of compositional variations on characteristics of coarse intermetallic particles in overaged 7000 aluminium alloys. Mater Sci Technol 2001;17(11):1324–8. https://doi.org/10.1179/026708301101509449.

[8] Starke EA, Staley JT. Application of modern aluminum alloys to aircraft. Prog Aerosp Sci 1996;32(2–3):131–72. https://doi.org/10.1016/0376-0421(95)00004-6.

[9] Senthil K, Iqbal MA, Chandel PS, Gupta N. Study of the constitutive behavior of 7075–T651 aluminum alloy. Int J Impact Eng 2017;108:171–90. https://doi.org/10.1016/J.IJIMPENG.2017.05.002.

[10] Garrett R, Lin J, Dean T. An investigation of the effects of solution heat treatment on mechanical properties for AA 6xxx alloys: Experimentation and modelling. Int J Plast 2005;21(8):1640–57. https://doi.org/10.1016/j.ijplas.2004.11.002.

[11] Krajewski PE, Schroth JG. Overview of Quick Plastic Forming Technology. Mater Sci Forum 2007;551–552:3–12. https://doi.org/10.4028/www.scientific.net/MSF.551-552.3.

[12] Huo W, Hou L, Zhang Y, Zhang J. Warm formability and post-forming microstructure/property of high-strength AA 7075–T6 Al alloy. Mater Sci Eng A 2016;675:44–54. https://doi.org/10.1016/J.MSEA.2016.08.054.

[13] Alistair DF, Dean TA, Jianguo L. Process for forming aluminium alloy sheet components. WO 2010/032002; 2009.

[14] Gao H, Weng T, Liu J, Li C, Li Z, Wang L, et al. Hot stamping of an Al-Li alloy: A feasibility study. MATEC Web Conf 2015;21:5007. https://doi.org/10.1051/matecconf/20152105007.

[15] Scharifi E, Knoth R, Weidig U. Thermo-mechanical forming procedure of high strength Aluminum sheet with improved mechanical properties and process efficiency. Procedia Manuf 2019;29. https://doi.org/10.1016/j.promfg.2019.02.165.

[16] Sajadifar SV, Scharifi E, Weidig U, Steinhoff K, Niendorf T. Effect of Tool Temperature on Mechanical Properties and Microstructure of Thermo-Mechanically Processed AA6082 and AA7075 Aluminum Alloys. HTM J Heat Treat Mater 2020;75:177–91. https://doi.org/10.3139/105.110412.

[17] MA W-y, WANG B-y, LIN J-G, TANG X-F. Influence of process parameters on properties of AA6082 in hot forming process. Trans Nonferrous Met Soc China 2017;27(11):2454–63. https://doi.org/10.1016/S1003-6326(17)60272-3.

[18] Scharifi E, Knoth R, Weidig U. Thermo-mechanical forming procedure of high strength Aluminum sheet with improved mechanical properties and process efficiency. Procedia Manuf 2019;29:481–9. https://doi.org/10.1016/J.PROMFG.2019.02.165.

[19] Shao ZT, Bai Q, Lin JG. A Novel Experimental Design to Obtain Forming Limit Diagram of Aluminium Alloys for Solution Heat Treatment, Forming and In-Die Quenching Process. Key Eng Mater 2014;622–623:241–8. https://doi.org/10.4028/www.scientific.net/KEM.622-623.241.

[20] Sajadifar SV, Scharifi E, Weidig U, Steinhoff K, Niendorf T. Performance of Thermo-Mechanically Processed AA7075 Alloy at Elevated Temperatures—From Microstructure to Mechanical Properties. Metals (Basel) 2020;10:884. https://doi.org/10.3390/met10070884.

[21] Scharifi E, Sajadifar SV, Moeini G, Weidig U, Böhm S, Niendorf T, et al. Dynamic Tensile Deformation of High Strength Aluminum Alloys Processed Following Novel Thermomechanical Treatment Strategies. Adv Eng Mater 2020;2000193. https://doi.org/10.1002/adem.202000193.

[22] Fan X, He Z, Yuan S, Lin P. Investigation on strengthening of 6A02 aluminum alloy sheet in hot forming-quenching integrated process with warm forming-dies. Mater Sci Eng A 2013;587:221–7. https://doi.org/10.1016/j.msea.2013.08.059.

[23] Sajadifar SV, Moeini G, Scharifi E, Lauhoff C, Böhm S, Niendorf T. On the Effect of Quenching on Postweld Heat Treatment of Friction-Stir-Welded Aluminum 7075 Alloy. J Mater Eng Perform 2019;28(8):5255–65. https://doi.org/10.1007/s11665-019-04252-3.

[24] Feng AH, Chen DL, Ma ZY. Microstructure and Cyclic Deformation Behavior of a Friction-Stir-Welded 7075 Al Alloy. Metall Mater Trans A 2010;41(4):957–71. https://doi.org/10.1007/s11661-009-0152-3.

[25] Nanninga N, White C, Furu T, Anderson O, Dickson R. Effect of orientation and extrusion welds on the fatigue life of an Al-Mg-Si-Mn alloy. Int J Fatigue 2008;30(9):1569–78. https://doi.org/10.1016/j.ijfatigue.2007.11.013.

[26] Winter L, Hockauf K, Winter S, Lampke T. Equal-channel angular pressing influencing the mean stress sensitivity in the high cycle fatigue regime of the 6082 aluminum alloy. Mater Sci Eng A 2020;795:140014. https://doi.org/10.1016/j.msea.2020.140014.

[27] Deng C, Wang H, Gong B, Li X, Lei Z. Effects of microstructural heterogeneity on very high cycle fatigue properties of 7050–T7451 aluminum alloy friction stir butt welds. Int J Fatigue 2016;83:100–8. https://doi.org/10.1016/j.ijfatigue.2015.10.001.

[28] Ghalehbandi SM, Fallahi-Arezodar A, Hosseini-Toudeshky H. Fatigue crack growth resistance of 7075 Al alloy after equal channel angular pressing. Fatigue Fract Eng Mater Struct 2016;39(12):1517–25. https://doi.org/10.1111/ffe.v39.1210.1111/ffe.12472.

[29] Leng L, Zhang ZJ, Duan QQ, Zhang P, Zhang ZF. Improving the fatigue strength of 7075 alloy through aging. Mater Sci Eng A 2018;738:24–30. https://doi.org/10.1016/j.msea.2018.09.047.

[30] Siddiqui RA, Abdul-Wahab SA, Pervez T. Effect of aging time and aging temperature on fatigue and fracture behavior of 6063 aluminum alloy under seawater influence. Mater Des 2008;29(1):70–9. https://doi.org/10.1016/j.matdes.2006.12.003.

[31] Hou LG, Xiao WL, Su H, Wu CM, Eskin DG, Katgerman L, et al. Room-temperature low-cycle fatigue and fracture behaviour of asymmetrically rolled high-strength 7050 aluminium alloy plates. Int J Fatigue 2021;142:105919. https://doi.org/10.1016/j.ijfatigue.2020.105919.

[32] Branco R, Costa JD, Borrego LP, Wu SC, Long XY, Antunes FV. Effect of tensile pre-strain on low-cycle fatigue behaviour of 7050–T6 aluminium alloy. Eng Fail Anal 2020;114:104592. https://doi.org/10.1016/j.engfailanal.2020.104592.

[33] Pandey V, Chattopadhyay K, Santhi Srinivas NC, Singh V. Role of ultrasonic shot peening on low cycle fatigue behavior of 7075 aluminium alloy. Int J Fatigue 2017;103:426–35. https://doi.org/10.1016/j.ijfatigue.2017.06.033.

[34] May A, Belouchrani MA, Taharboucht S, Boudras A. Influence of heat treatment on the fatigue behaviour of two aluminium alloys 2024 and 2024 plated. Procedia Eng., vol 2, Elsevier; 2010, p. 1795–804. Doi: 10.1016/j.proeng.2010.03.193.

[35] Shou WB, Yi DQ, Liu HQ, Tang C, Shen FH, Wang B. Effect of grain size on the fatigue crack growth behavior of 2524–T3 aluminum alloy. Arch Civ Mech Eng 2016;16(3):304–12. https://doi.org/10.1016/j.acme.2016.01.004.

[36] Yin D, Liu H, Chen Y, Yi D, Wang B, Wang B, et al. Effect of grain size on fatigue-crack growth in 2524 aluminium alloy. Int J Fatigue 2016;84:9–16. https://doi.org/10.1016/j.ijfatigue.2015.11.011.

[37] Fu X, Zhang J, Lin J. Study on the fatigue life and damage accumulation of a compressor blade based on a modified nonlinear damage model. Fatigue Fract Eng Mater Struct 2018;41(5):1077–88. https://doi.org/10.1111/ffe.v41.510.1111/ffe.12753.

[38] Ren XD, Zhan QB, Yang HM, Dai FZ, Cui CY, Sun GF, et al. The effects of residual stress on fatigue behavior and crack propagation from laser shock processing-worked hole. Mater Des 2013;44:149–54. https://doi.org/10.1016/j.matdes.2012.07.024.

[39] Liu K, Mirza F, Chen X. Effect of Overaging on the Cyclic Deformation Behavior of an AA6061 Aluminum Alloy. Metals (Basel) 2018;8:528. https://doi.org/10.3390/met8070528.

[40] Niendorf T, Lotze C, Canadinc D, Frehn A, Maier HJ. The role of monotonic pre-deformation on the fatigue performance of a high-manganese austenitic TWIP steel. Mater Sci Eng A 2009;499(1–2):518–24. https://doi.org/10.1016/

j.msea.2008.09.033.
[41] Picak S, Wegener T, Sajadifar SV, Sobrero C, Richter J, Kim H, et al. On the low cycle fatigue response of CoCrNiFeMn high entropy alloy with ultra-fine grain structure. Acta Mater 2021;205:116540. https://doi.org/10.1016/j.actamat.2020.116540.
[42] Wegener T, Haase C, Liehr A, Niendorf T. On the influence of ϰ-carbides on the low-cycle fatigue behavior of high-Mn light-weight steels. Int J Fatigue 2021;150:106327. https://doi.org/10.1016/j.ijfatigue.2021.106327.
[43] Wegener T, Brenne F, Fischer A, Möller T, Hauck C, Auernhammer S, et al. On the structural integrity of Fe-36Ni Invar alloy processed by selective laser melting. Addit Manuf 2021;37:101603. https://doi.org/10.1016/j.addma.2020.101603.
[44] Starink MJ. Reduced fracturing of intermetallic particles during crack propagation in age hardening Al-based alloys due to PFZs. Mater Sci Eng A 2005;390(1–2):260–4. https://doi.org/10.1016/j.msea.2004.09.053.
[45] Rhodes CG, Mahoney MW, Bingel WH, Spurling RA, Bampton CC. Effects of friction stir welding on microstructure of 7075 aluminum. Scr Mater 1997;36(1):69–75. https://doi.org/10.1016/S1359-6462(96)00344-2.
[46] Scharifi E, Savaci U, Kavaklioglu ZB, Weidig U, Turan S, Steinhoff K. Effect of thermo-mechanical processing on quench-induced precipitates morphology and mechanical properties in high strength AA7075 aluminum alloy. Mater Charact 2021;174:111026. https://doi.org/10.1016/j.matchar.2021.111026.
[47] Kim Y, Hwang W. High-cycle, low-cycle, extremely low-cycle fatigue and monotonic fracture behaviors of low-carbon steel and itswelded joint. Materials (Basel) 2019;12:4111. https://doi.org/10.3390/MA12244111.
[48] Sajadifar SV, Yapici GG, Demler E, Krooß P, Wegener T, Maier HJ, et al. Cyclic deformation response of ultra-fine grained titanium at elevated temperatures. Int J Fatigue 2019;122:228–39. https://doi.org/10.1016/j.ijfatigue.2019.01.021.
[49] Shao CW, Zhang P, Liu R, Zhang ZJ, Pang JC, Duan QQ, et al. A remarkable improvement of low-cycle fatigue resistance of high-Mn austenitic TWIP alloys with similar tensile properties: Importance of slip mode. Acta Mater 2016;118:196–212. https://doi.org/10.1016/j.actamat.2016.07.034.
[50] Desmukh MN, Pandey RK, Mukhopadhyay AK. Effect of aging treatments on the kinetics of fatigue crack growth in 7010 aluminum alloy. Mater Sci Eng A 2006;435–436:318–26. https://doi.org/10.1016/J.MSEA.2006.07.063.
[51] Chen X, Liu Z, Xia P, Ning A, Zeng S. Transition of crack propagation from a transgranular to an intergranular path in an overaged Al-Zn-Mg-Cu alloy during cyclic loading. Met Mater Int 2013;19(2):197–203. https://doi.org/10.1007/s12540-013-2009-y.
[52] Suresh S. Fatigue of Materials. 2nd Ed. Cambridge, UK: Cambridge University Press; 1998.
[53] Christ H-J, Mughrabi H. Cyclic stress-strain response and microstructure under variable amplitude loading. Fatigue Fract Eng Mater Struct 1996;19(2–3):335–48. https://doi.org/10.1111/j.1460-2695.1996.tb00971.x.
[54] Christ H-J, Lades K, Völkl L, Mughrabi H. The Role of Microstructural Processes in the Application of the Incremental Step Test to Determine the Cyclic Stress-Strain Curve of an Aluminium Alloy. Low Cycle Fatigue Elasto-Plastic Behav Mater, Springer Netherlands; 1992, p. 100–5. Doi: 10.1007/978-94-011-2860-5_16.
[55] Picak S, Wegener T, Sajadifar SV, Sobrero C, Richter J, Kim H, et al. On the Low Cycle Fatigue Response of CoCrNiFeMn High Entropy Alloy with Ultra-fine Grain Structure. Acta Mater 2020. https://doi.org/10.1016/j.actamat.2020.116540.
[56] Christ H-J. Ermüdungsverhalten metallischer Werkstoffe. Weinheim: Wiley-VCH; 2009.
[57] Mohamed A, El-Madhoun Y, Bassim MN. Dislocation boundary width changes due to cyclic hardening. Metall Mater Trans A Phys Metall Mater Sci, vol. 37, Springer; 2006, p. 3441–3. Doi: 10.1007/s11661-006-1039-1.
[58] El-Madhoun Y, Mohamed A, Bassim MN. Cyclic stress-strain response and dislocation structures in polycrystalline aluminum. Mater Sci Eng A 2003;359(1–2):220–7. https://doi.org/10.1016/S0921-5093(03)00347-2.
[59] Farrahi GH, Ghodrati M, Azadi M, Rezvani Rad M. Stress–strain time-dependent behavior of A356.0 aluminum alloy subjected to cyclic thermal and mechanical loadings. Mech Time-Dependent Mater 2014;18(3):475–91. https://doi.org/10.1007/s11043-014-9238-4.
[60] Moeini G, Sajadifar SV, Wegener T, Brenne F, Niendorf T, Böhm S. On the low-cycle fatigue behavior of friction stir welded Al–Si12 parts produced by selective laser melting. Mater Sci Eng A 2019;764:138189. https://doi.org/10.1016/j.msea.2019.138189.
[61] Lambers H-G, Rüsing CJ, Niendorf T, Geissler D, Freudenberger J, Maier HJ. On the low-cycle fatigue response of pre-strained austenitic Fe61Mn24Ni6.5Cr8.5 alloy showing TWIP effect. Int J Fatigue 2012;40:51–60. https://doi.org/10.1016/j.ijfatigue.2012.01.002.
[62] Niendorf T, Wegener T, Li Z, Raabe D. Unexpected cyclic stress-strain response of dual-phase high-entropy alloys induced by partial reversibility of deformation. Scr Mater 2018;143:63–7. https://doi.org/10.1016/J.SCRIPTAMAT.2017.09.013.
[63] Niendorf T, Canadinc D, Maier HJ. Fatigue Damage Evolution in Ultrafine-Grained Interstitial-Free Steel. Adv Eng Mater 2011;13(4):275–80. https://doi.org/10.1002/adem.v13.410.1002/adem.201000272.
[64] Mughrabi H. Microstructural mechanisms of cyclic deformation, fatigue crack initiation and early crack growth. Philos Trans R Soc A Math Phys Eng Sci 2015;373(2038):20140132. https://doi.org/10.1098/rsta.2014.0132.
[65] Mughrabi H. Microstructural fatigue mechanisms: Cyclic slip irreversibility, crack initiation, non-linear elastic damage analysis. Int J Fatigue 2013;57:2–8. https://doi.org/10.1016/j.ijfatigue.2012.06.007.
[66] Tian DD, Liu XS, He GQ, Shen Y, Lv SQ, Wang QG. Low cycle fatigue behavior of casting A319 alloy under two different aging conditions. Mater Sci Eng A 2016;654:60–8. https://doi.org/10.1016/j.msea.2015.12.023.
[67] Nix KJ, Flower HM. The micromechanisms of fatigue crack growth in a commercial Al-Zn-Mg-Cu alloy. Acta Metall 1982;30(8):1549–59. https://doi.org/10.1016/0001-6160(82)90175-4.
[68] McMillan JC, Pelloux RM. Fatigue crack propagation under programmed loads and crack tip opening displacements. Eng Fract Mech 1970;2(1):81–4. https://doi.org/10.1016/0013-7944(70)90031-7.
[69] Zhang JZ. A shear band decohesion model for small fatigue carck growth in an ultra-fine grain aluminium alloy. Eng Fract Mech 2000;65(6):665–81. https://doi.org/10.1016/S0013-7944(99)00148-4.
[70] Feltner CE, Laird C. Cyclic stress-strain response of F.C.C. metals and alloys-I Phenomenological experiments. Acta Metall 1967;15(10):1621–32. https://doi.org/10.1016/0001-6160(67)90137-X.
[71] Quesnel DJ, Tsou JC. A quantitative approach to the cell shuttling model. Mater Sci Eng 1983;59(1):91–8. https://doi.org/10.1016/0025-5416(83)90091-5.
[72] Tu S-T, Zhang X-C. Fatigue Crack Initiation Mechanisms. Ref. Modul. Mater. Sci. Mater. Eng., Elsevier 2016. https://doi.org/10.1016/b978-0-12-803581-8.02852-6.
[73] Serrano-Munoz I, Buffiere JY, Mokso R, Verdu C, Nadot Y. Location, location & size: Defects close to surfaces dominate fatigue crack initiation. Sci Rep 2017;7:1–9. https://doi.org/10.1038/srep45239.
[74] Mughrabi H. Cyclic slip irreversibilities and the evolution of fatigue damage. Metall Mater Trans B Process Metall Mater Process Sci 2009;40(4):431–53. https://doi.org/10.1007/s11663-009-9240-4.
[75] Weidner A, Man J, Tirschler W, Klapetek P, Blochwitz C, Polák J, et al. Half-cycle slip activity of persistent slip bands at different stages of fatigue life of polycrystalline nickel. Mater Sci Eng A 2008;492(1–2):118–27. https://doi.org/10.1016/j.msea.2008.03.027.
[76] Mughrabi H. On, “multi-stage” fatigue life diagrams and the relevant life-controlling mechanisms in ultrahigh-cycle fatigue. Fatigue Fract Eng Mater Struct 2002;25:755–64. https://doi.org/10.1046/j.1460-2695.2002.00550.x.